




Article

# Preparation of Magnetic Iron Oxide Incorporated Mesoporous Silica Hybrid Composites for pH and Temperature-Sensitive Drug Delivery

Madhappan Santhamoorthy <sup>1,†</sup>, Kokila Thirupathi <sup>2,†</sup>, Selvakumar Krishnan <sup>3</sup>, Loganathan Gunganathan <sup>4</sup> , Sushma Dave <sup>5</sup> , Thi Tuong Vy Phan <sup>6,7,\*</sup>  and Seong-Cheol Kim <sup>1,\*</sup>

<sup>1</sup> School of Chemical Engineering, Yeungnam University, Gyeongsan 38541, Republic of Korea

<sup>2</sup> Department of Physics, Government Arts and Science College for Women, Karimangalam, Dharmapuri 635111, Tamil Nadu, India

<sup>3</sup> Department of Physics, Bannari Amman Institute of Technology, Sathyamangalam, Erode 638401, Tamil Nadu, India

<sup>4</sup> Department of Physics, Annamalai University, Annamalai Nagar, Chidambaram 608002, Tamil Nadu, India

<sup>5</sup> Department of Applied Sciences, JIET, Jodhpur 342802, Rajasthan, India

<sup>6</sup> Center for Advanced Chemistry, Institute of Research and Development, Duy Tan University, 03 Quang Trung, Hai Chau, Danang 550000, Vietnam

<sup>7</sup> Faculty of Environmental and Chemical Engineering, Duy Tan University, 03 Quang Trung, Hai Chau, Danang 550000, Vietnam

\* Correspondence: phanttuongvy4@duytan.edu.vn (T.T.V.P.); sckim07@yu.ac.kr (S.-C.K.); Tel.: +82-53-810-2787 (S.-C.K.)

† These authors contributed equally to this work.

**Abstract:** In clinical applications for cancer treatment, chemotherapy coupled with thermotherapy is highly considered. The development of multifunctional nanocomposite materials is an appealing strategy for use in various applications including biomedical applications. We present the preparation of dopamine-modified mesoporous silica material, in which magnetic iron oxide nanoparticles (FeNP) were grown onto the outer surface via the complexation of iron (Fe(III) and Fe(II)) ions with the dopamine groups modified on the silica hybrid and subsequent chemical reduction approaches. The prepared magnetic iron oxide incorporated with mesoporous silica hybrid composite nanoparticles (FeNP@MSHC NPs) had a large surface area (346 m<sup>2</sup>/g), pore size (3.2 nm), and pore volume (0.048 cm<sup>3</sup>/g). The formation of FeNP on the outer surface of the FeNP@MSHC NPs results in superparamagnetic characteristics. Furthermore, the prepared FeNP@MSHC NPs have a high drug (Dox) loading capacity (~62%) as well as pH- and temperature-responsive drug release efficiency. In addition, the MTT assay result shows the biocompatibility of the prepared FeNP@MSHC NPs. As a result, the FeNP@MSHC NPs could be utilized in cancer treatment for pH and temperature-sensitive delivery of chemotherapeutic agents to the target sites.

**Keywords:** magnetic iron oxide nanoparticles; mesoporous silica hybrid; pH stimuli; drug delivery; cell viability



**Citation:** Santhamoorthy, M.; Thirupathi, K.; Krishnan, S.; Gunganathan, L.; Dave, S.; Phan, T.T.V.; Kim, S.-C. Preparation of Magnetic Iron Oxide Incorporated Mesoporous Silica Hybrid Composites for pH and Temperature-Sensitive Drug Delivery. *Magnetochemistry* **2023**, *9*, 81. <https://doi.org/10.3390/magnetochemistry9030081>

Academic Editor: Karim Zehani

Received: 19 February 2023

Revised: 5 March 2023

Accepted: 10 March 2023

Published: 12 March 2023



**Copyright:** © 2023 by the authors. Licensee MDPI, Basel, Switzerland. This article is an open access article distributed under the terms and conditions of the Creative Commons Attribution (CC BY) license (<https://creativecommons.org/licenses/by/4.0/>).

## 1. Introduction

Recently, researchers have been focusing on developing nanomaterials that integrate two or more functionalities to improve efficiency [1–3]. The nanomaterials are attracting much research attention due to their unique physicochemical properties as well as their practical usefulness in a range of applications including drug/gene delivery [4–8]. Ordered mesoporous silica nanoparticles are thought to be promising among the materials used for various applications because of their physicochemical structural characteristics and cell compatibility [9–12]. Organofunctional units introduced into silica nanoparticles may extend their uses in various applications [13–17].

The mesoporous silicas with magnetic nanoparticles have recently gained more attention from researchers due to their non-toxicity, biodegradability, ease of separation by an external magnetic field, as well as their recyclability [18–20]. As a result, much effort has been put into developing magnetic silica materials for a wide range of applications [21–23]. Magnetic nanoparticles incorporated with mesoporous silica nanoparticles have advantages such as allowing for high loading efficiency of payloads. In addition, fast accumulation kinetics can be achieved, and it could be directed to the target sites by applying an external magnetic field. The formation of small magnetic nanoparticles on the silica surfaces via metal–ligand complexation could be regarded as a simple method for producing magnetic silica composites [24,25]. Because magnetic nanoparticles are present on the exterior surfaces, the internal mesopore channels remain vacant, allowing them to access a wide range of cargoes. Moreover, the magnetic nanoparticles on the outer surface of silicas can improve heating capacity when applying an external magnetic field [26,27].

The stimuli-responsive nanoparticle-based drug delivery system is regarded as a promising cancer treatment platform because these nanomaterials react to internal and exterior stimuli such as pH, enzymes, and temperature [28]. pH stimulus is regarded to be the most effective of all stimuli due to the pH difference in the body between normal cells and cancerous sites. Most tumor tissues have an acidic pH as compared to normal cells, which facilitates selective drug release [29]. Concurrent administration of drugs and intracellular hyperthermic heat into tumor tissues can considerably increase the synergistic benefits of chemotherapy [30]. The magnetic mesoporous silica-based drug delivery technology has the unique advantage of allowing nanoparticles to be injected into the body and accumulated at specific sites by an external magnetic field. As a consequence, the nanocarrier can efficiently release the therapeutic agents to specific sites while causing no harm to healthy cells [31]. The pH-responsive nanocarriers can effectively retain the loaded drugs under physiological pH and deliver them under acidic pH environments. Temperature stimulation can also increase drug molecule solubility and diffusion rate from the drug carrier system.

This work proposed the preparation of a magnetic mesoporous silica hybrid nanocarrier by growing magnetic iron oxide (FeNP) nanoparticles on the outer silica surfaces using a metal–ligand complexation and chemical reduction technique. To begin, mesoporous silica nanoparticles were created by sol-gel co-condensing a dopamine-silane (DP) precursor and a silica source, tetraethyl orthosilicate (TEOS). Second, the exterior silica surface of the as-synthesized samples was modified with DP precursor. Finally, magnetic iron oxide nanoparticles were produced on the outer surface of silica particles by introducing ferric ( $\text{Fe}^{3+}$ ) and ferrous ( $\text{Fe}^{2+}$ ) ion solutions, followed by chemical reduction. Doxorubicin (Dox) was employed to assess the drug loading and delivery efficiency of the produced magnetic mesoporous silica hybrid composite nanoparticles (FeNP@MSHC NPs) at pH 7.4 and 5.0 and temperatures of 25 °C and 42 °C, respectively. Further, the *in vitro* cell compatibility and cell-uptake behavior of the prepared FeNP@MSHC NPs were also determined using MDA-MB-231 cells.

## 2. Materials and Methods

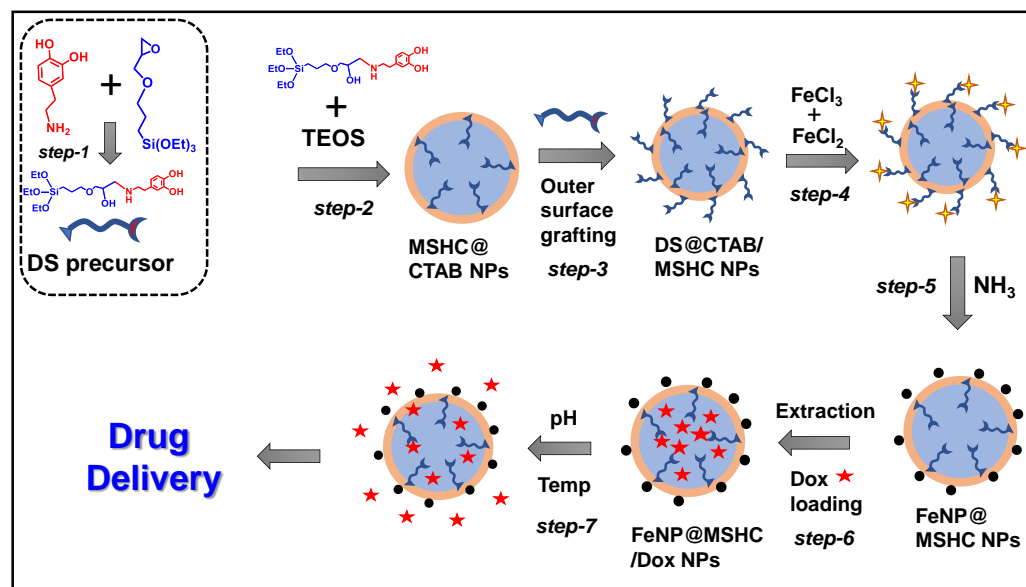
### 2.1. Reagents

Tetraethyl orthosilicate (TEOS, 98%), (3-glycidyloxypropyl)trimethoxysilane (GPTMS, 95%), iron(III) chloride ( $\text{FeCl}_3$ , 97%), iron(II) chloride ( $\text{FeCl}_2$ , 98%), dopamine hydrochloride (98%), ammonium hydroxide (28%), doxorubicin hydrochloride (Dox), tetrahydrofuran (THF, 99%), were purchased from Aldrich Chemicals. All the chemicals were used as received.

### 2.2. Synthesis of Dopamine-Silane (DS) Precursor

To synthesize the dopamine-silane precursor, 0.5 g (3.2 mmol) of dopamine hydrochloride was dissolved in a 100 mL round-bottomed flask with 50 mL of anhydrous THF. Approximately 0.8 g (3.2 mmol) of GPTMS was added to this under vigorous stirring in a

nitrogen environment at 45 °C for 24 h (Scheme 1, step 1). After the reaction was completed, the product was concentrated and purified further using hexane. Vacuum drying was used to dry the resulting viscous mass.  $^1\text{H}$  NMR (400 MHz,  $\text{CDCl}_3$ ):  $\delta$ 0.42 (t, 4 H,  $\text{SiCH}_2$ ),  $\delta$ 1.05 (t, 18 H,  $\text{CH}_2\text{CH}_2\text{O}$ ),  $\delta$ 1.59 (t, 4H,  $\text{SiCH}_2\text{CH}_2$ ),  $\delta$ 3.62 (t, 4H, NH),  $\delta$ 6.4–7.2 (m, 18 H, aromatic) (Figure 1a).



**Scheme 1.** Schematic representation for the synthesis of dopamine-silane precursor (step 1); synthesis of MSHC@CTAB NPs (step 2); surface grafting of DS precursor onto the outer surface of DS@MSHC@CTAB NPs (step 3); Fe(III) complexation with DS precursor (step 4); formation of FeNP by chemical reduction (step 5); surfactant extraction and Dox loading into the FeNP@MSHC NPs (step 6); and pH- and temperature-stimuli-responsive drug delivery (step 7).

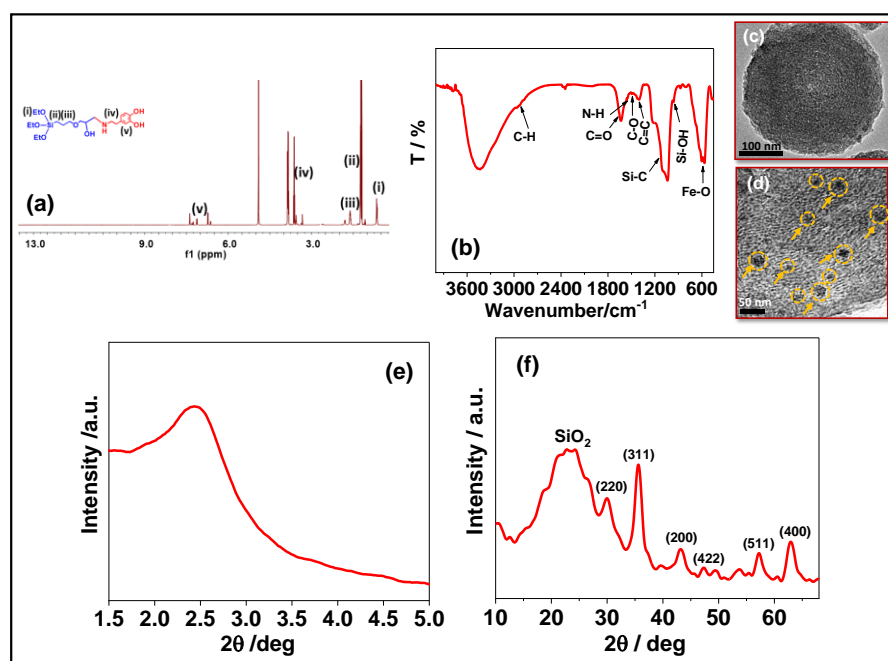


**Figure 1.** (a)  $^1\text{H}$  NMR spectrum of DS precursor; (b) FTIR spectrum; (c,d) TEM images and the yellow circles indicate the presence of magnetic iron oxide nanoparticles; (e,f) low and higher angle XRD spectra of the FeNP@MSHC NPs.

### 2.3. Synthesis of Dopamine-Silane Integrated with Mesoporous Silica Nanoparticles

To create a dopamine-silane precursor integrated with mesoporous silica nanoparticles, sol-gel hydrolysis and a co-condensation approach were used [32]. Under magnetic stirring, about 1 g of CTAB was dissolved in 180 mL of deionized water containing ammonia solution (3 g). The premixed solution of DS precursor (20 mol%) and TEOS (80 mol%) was gently introduced into the surfactant solution under strong magnetic stirring once the solution became clear. The resulting mixture was then stirred for 24 h at 40 °C and another 24 h at 85 °C. The obtained product was filtered, rinsed with water and ethanol, and dried at 60 °C. The as-prepared sample was labeled MSHC@CTAB NPs (Scheme 1, step 2).

### 2.4. Synthesis of Iron Oxide NPs Incorporated Mesoporous Silica Composite Nanoparticles (FeNP@MSHC NPs)

To produce magnetic iron oxide nanoparticles on the as-made DS@MSHC@CTAB NPs' outer surface, the DS@MSHC@CTAB NPs were first modified with DS precursor units. To do so, 0.5 g of as-made DS@MSHC@CTAB NPs sample was dispersed in 50 mL dry toluene, and 5 mL (0.2 M) of DS precursor solution was added under reflux conditions at 80 °C for 24 h. The obtained suspension was filtered, washed with toluene and ethanol, and dried at 60 °C. (Scheme 1, step 3). The magnetic iron oxide nanoparticles were formed on the outer surface of the DS@MSHC@CTAB NPs in the next step by dispersing them (0.5 g) in 250 mL deionized water. A mixture of iron precursor was introduced as follows. First, 50 mg (0.07 mmol) of FeCl<sub>3</sub> solution was gently added for 15 min during magnetic stirring to produce a Fe(III)-dopamine complex on the outer surface of the DS@MSHC@CTAB NPs (Scheme 1, step 4) [33]. Following that, 50 mg (0.07 mmol) of FeCl<sub>2</sub> solution was added under magnetic stirring for 30 min, followed by 5 mL of ammonia solution under strong magnetic stirring to generate magnetic iron oxide nanoparticles (FeNP) on the outer surface of the DS@MSHC@CTAB NPs (Scheme 1, step 5). Finally, using an alcoholic ammonium nitrate solution, the occluded CTAB was removed from the magnetic iron oxide nanoparticles produced samples. To carry out this procedure, 0.5 g of DS@MSHC@CTAB NPs sample (0.5 g) was dispersed in 200 mL deionized water, and alcoholic ammonium nitrate solution (25 mL) was added while strong magnetic stirring was carried out at 60 °C for 12 h. The extraction procedure was performed three times before being dried at 60 °C. The magnetic iron oxide nanoparticles modified with dopamine silane functionalized mesoporous silica composite nanoparticles were labeled as FeNP@MSHC NPs (Scheme 1, step 6).

### 2.5. Characterization

The X-ray diffraction (XRD) patterns were measured on X'Pert-MPD system (Philips, Almelo, The Netherlands) X-ray diffractometer with Cu K $\alpha$  radiation. N<sub>2</sub> adsorption-desorption isotherms were measured at a liquid nitrogen temperature (−196 °C) using a Nova 4000e surface area analyzer. The specific surface area was calculated by the Brunauer-Emmett-Teller (BET) method. The magnetic behavior of the sample was analyzed by using a superconducting quantum interference device (SQUID) at 300 K on a quantum design vibrating sample magnetometer (VSM) (MPMS XL, 7.0). Transmission electron microscopy (TEM) was performed on JEOL JEM-2100F at 200 kV.

### 2.6. Drug Loading into the FeNP@MSHC NPs

Dox was employed to investigate the drug-loading behavior of the FeNP@MSC NPs. For drug loading, 100 mg of FeNP@MSHC NPs were ultrasonically dispersed in Dox solution (5 mL, 1 mg/mL ethanol) for 5 min before being magnetically stirred for 24 h. Finally, the sample was centrifuged and rinsed with 1 mL of water to remove surface adherent drug molecules. The drug-loaded sample was labeled FeNP@MSHC/Dox NPs (Scheme 1, step 6). The washing solution was collected to assess the drug encapsulation using UV-vis spectrometry as follows. Drug loading (%) = Wt. of the drug in sample/Wt.

of drug injected  $\times 100$ . The FeNP@MSHC/Dox NPs were estimated to have a maximum drug loading of approximately ~62%.

### 2.7. Drug Release Study from the FeNP@MSHC/Dox NPs

In vitro drug delivery experiments were carried out at different settings, including (i) variable pH (pH 7.4 and 5.0); (ii) varied temperature (25 °C and 42 °C); and the combined pH and temperature (pH 7.4/42 °C and pH 5.0/42 °C). To investigate the drug delivery performance of the prepared FeNP@MSHC/Dox NPs, about 100 mg of Dox-loaded FeNP@MSHC/Dox NPs were taken in a dialysis bag (MWCO 12 kDa) and immersed in 20 mL of PBS medium with a predetermined pH setting while magnetic stirring was performed. UV-vis spectrometric measurement at 498 nm was used to monitor the Dox release from the FeNP@MSHC/Dox NPs. For this measurement, 1 mL of the buffer medium containing the released drug was taken at a predetermined time and analyzed with a UV-vis spectrometer.

### 2.8. MTT Assay Analysis of the FeNP@MSHC/Dox NPs

MDA-MB-231 cells were used to test the cell compatibility of the prepared FeNP@MSHC NPs and FeNP@MSHC/Dox NPs, respectively. To perform this study, cells were grown in 96-well plates ( $1 \times 10^4$  cells/well) with Dulbecco's modified eagle's medium (DMEM) at 37 °C for these studies. The FeNP@MSHC/Dox NPs sample was then exposed to the cultivated cells at various doses and incubated for 24 h. After 24 h, about 20  $\mu$ L of the MTT solution was used to dissolve the formazan crystals in each well and then the optical density (OD) was evaluated at 570 nm. Cell viability was determined as follows [34]. Cell viability (%) =  $OD_{\text{treated}} / OD_{\text{control}} \times 100$ , where  $OD_{\text{treated}}$ : the cells exposed with the FeNP@MSHC NPs and FeNP@MSHC/Dox NPs, respectively. The  $OD_{\text{control}}$ : only control cells without sample.

### 2.9. Cell-Uptake Study

MDA-MB-231 cells were used to examine the cell uptake of FeNP@MSHC/Dox NPs. For this experiment, FeNP@MSHC/Dox NPs (10  $\mu$ g/mL) were exposed to MDA-MB-231 cells for 5 h. The cells were then rinsed with a cold PBS solution to eliminate surface-adhered particles. The cells were then fixed for 15 min in a 4% paraformaldehyde solution. Finally, the cells were examined using a fluorescence spectrophotometer.

## 3. Results and Discussion

### 3.1. Characterization of the FeNP@MSHC NPs

The presence of dopamine-silane functional groups in the FeNP@DS@MSC NPs was verified by FTIR analysis. The FTIR spectrum of FeNP@MSHC NPs is shown in Figure 1a. The vibration bands at 1060  $\text{cm}^{-1}$  and 961  $\text{cm}^{-1}$ , as shown in Figure 1a, were ascribed to Si-O-Si and hydroxyl groups, respectively [35]. The broad band appeared around 3442  $\text{cm}^{-1}$  indicating the stretching modes of hydroxyl (Si-OH) groups. The alkyl C-H band for the alkyl chains present in the existing dopamine-silane functional units was shown by the bands at 2959  $\text{cm}^{-1}$  and 2867  $\text{cm}^{-1}$ . Furthermore, the carbonyl (-C=O) and amine (-N-H) groups have stretching peaks at 1489  $\text{cm}^{-1}$  and 1558  $\text{cm}^{-1}$ , respectively, while the aromatic dopamine groups have C-O and C=C vibrations at 1423  $\text{cm}^{-1}$  and 1394  $\text{cm}^{-1}$ . Furthermore, the typical vibration band for Fe-O stretching emerged around 567  $\text{cm}^{-1}$ , suggesting the presence of magnetic iron oxide nanoparticles in the FeNP@MSHC NPs [36]. The presence of organosilane functionalities and magnetic iron oxide nanoparticles in the FeNP@MSHC NPs is confirmed by FTIR data.

Figure 1b,c depicts TEM images of the FeNP@MSHC NPs. The formation of mesopores in the FeNP@MSHC NPs was confirmed by TEM image (Figure 1b), and the presence of magnetic iron oxide nanoparticles on the FeNP@MSHC NPs was visualized from the dark black spots indicated in arrows (Figure 1c), indicating that the FeNPs were formed by the chemical reduction process. The sample consists of several individual iron oxide

nanoparticles on the FeNP@MSHC NPs with an average particle size of about 5–10 nm. The low-angle XRD pattern of the FeNP@MSHC NPs is shown in Figure 1d. As shown in Figure 1d, the FeNP@MSHC NPs exhibit a diffraction peak at  $2\theta = 2.4^\circ$ , indicating the formation of mesopores. Further, the higher angle XRD pattern shows a broad peak at  $2\theta = 20\text{--}30^\circ$ , suggesting the presence of silica matrix, and the diffraction peaks at  $2\theta = 29.6^\circ$ ,  $35.2^\circ$ ,  $43.4^\circ$ ,  $47.2^\circ$ ,  $57.3^\circ$ , and  $63.5^\circ$  were indicated to [220], [311], [400], [422], [511] and [440] reflection planes which evidenced the presence of magnetic iron oxide crystals in the FeNP@MSHC NPs (Figure 1e) [37].

Figure 2a,b shows the nitrogen sorption isotherm and pore size distribution curves of the FeNP@MSHC NPs. As shown in Figure 2a, FeNP@MSHC NPs exhibit a type IV isotherm, representing the formation of mesoporous silica nanoparticles. The FeNP@MSHC NPs' estimated surface area, pore size, and mesopore volume were estimated to be approximately  $346\text{ m}^2/\text{g}$ ,  $3.2\text{ nm}$ , and  $0.048\text{ cm}^3/\text{g}$ , respectively (Figure 2b) (Table 1). The surface charge of the FeNP@MSHC NPs was determined using the zeta potential measurement. As shown in Figure 2c, the FeNP@MSHC NPs had a little positive zeta potential value of around  $+10.3\text{ mV}$  at pH 4 and a negative zeta potential value of about  $-36\text{ mV}$  at pH 10. The positive zeta potential was detected due to the protonation of amine groups present in the FeNP@MSHC NPs, confirming that the FeNP@MSHC NPs contain dopamine-silane functional groups (Figure 2c). Furthermore, the particle size of the FeNP@MSHC NPs was determined using the dynamic light scattering (DLS) technique. As indicated in Figure 2d, the average particle size of the FeNP@MSHC NPs was estimated to be between 100 and 400 nm.

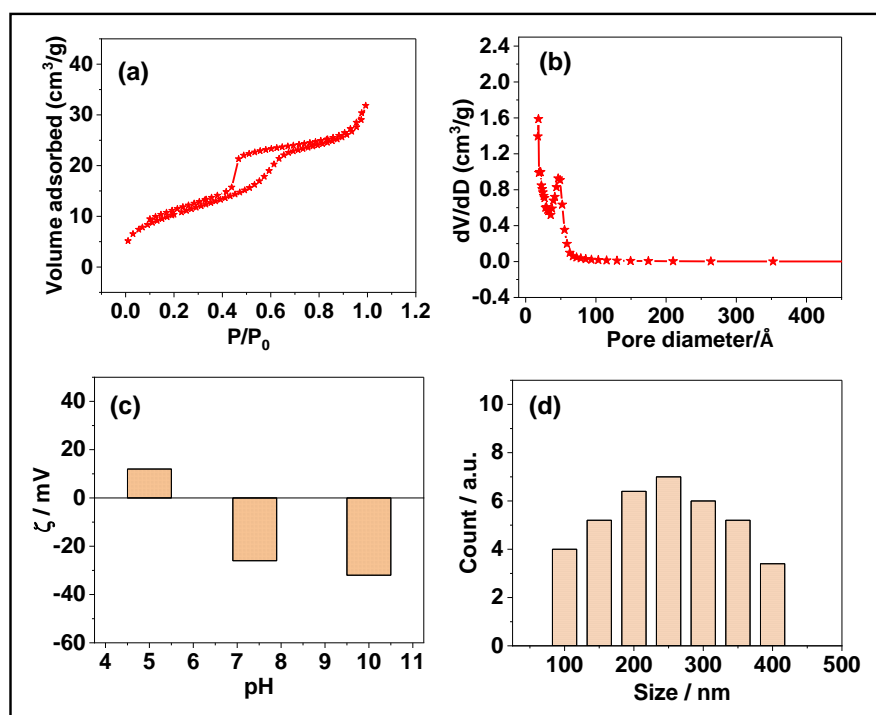


**Figure 2.** (a) N<sub>2</sub> adsorption-desorption; (b) pore size distributions; (c) zeta potential measurement; and (d) particle size distributions of the FeNP@MSHC NPs.

**Table 1.** Mesopore properties of FeNP@MSHC NPs.

Sample	Surface Area (m <sup>2</sup> /g)	Pore Size (nm)	Pore Volume (cm <sup>3</sup> /g)	Dox Loading (%)
FeNP@MSHC NPs	364 ± 2.5	3.2 ± 0.1	0.048 ± 1.5	~62 ± 1.5

The thermal stability of the prepared FeNP@MSHC NPs was determined by thermogravimetric (TG) analysis. Figure 3a shows a first weight loss of around 1.8 wt.% occurs at about 100 °C, suggesting physisorbed moisture evaporation. Furthermore, the second stage weight loss of around 17.5 wt.% occurs at 101–650 °C, implying the decomposition of the integrated dopamine-silane functional groups in the FeNP@MSHC NPs. Furthermore, the last weight loss occurs above 650 °C owing to inorganic matrix degradation. The TGA results revealed that a significant amount (17.5 wt.%) of organic functionalities were included in the FeNP@MSHC NPs. The magnetic properties of the FeNP@MSHC NPs were investigated using a superconducting quantum interference device (SQUID) and a vibrating sample magnetometer (VSM). As shown in Figure 3b, the magnetization curve of the FeNP@MSHC NPs revealed a magnetic saturation value of around 18.5 emu/g. Furthermore, the absence of significant hysteresis in the room temperature magnetization curve of the FeNP@MSHC NPs shows that the synthesized FeNP@MSHC NPs exhibit superparamagnetic behavior (Figure 3c) [38]. The magnetic behavior of the magnetic iron oxide particles present in the FeNP@MSHC NPs was further verified by dispersing about 10 mg of FeNP@MSHC NPs in PBS medium under ultrasonication and then kept near a bar magnet.

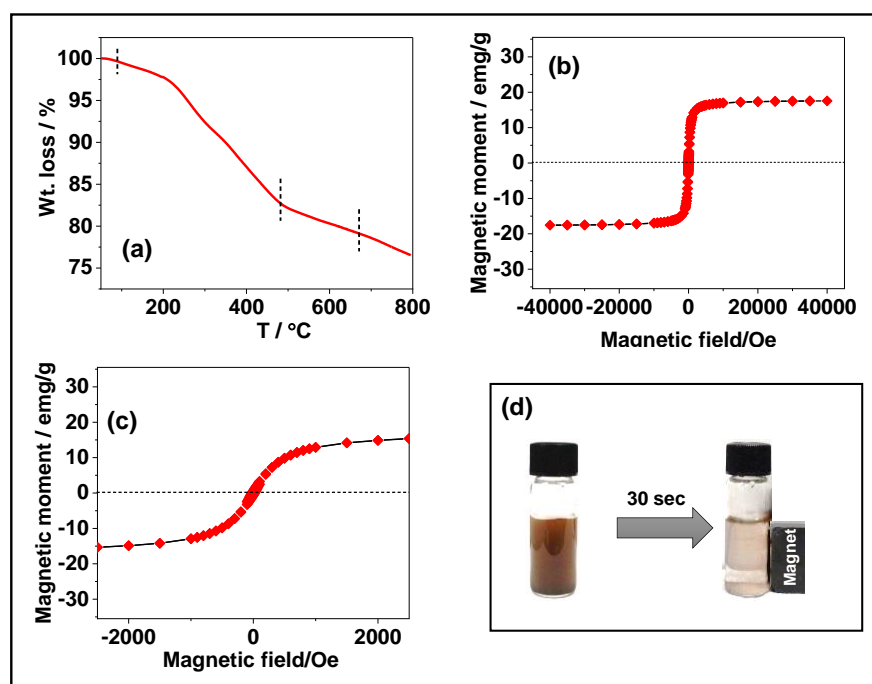


**Figure 3.** (a) TGA curve; (b,c) magnetization curve of FeNP@MSHC NPs. (d) The photographic image shows the attraction of FeNP@MSHC NPs by external magnetic field.

When the bar magnet was positioned near the glass vial, the sample attracted quickly to the external magnet bar (Figure 3d, inset). This study demonstrated that magnetic iron oxide nanoparticles were formed on the FeNP@MSHC NPs and could be directed by an external magnetic field, indicating that the FeNP@MSHC NPs are suitable for target drug delivery applications driven by an external magnetic field.

### 3.2. Drug Loading into the FeNP@MSHC NPs

The integrated dopamine functionalities present inside the FeNP@MSHC NPs' mesopore channels serve as drug-binding sites for the loaded drugs. To assess the drug loading of the FeNP@MSHC NPs, the anticancer agent Dox was utilized. Dox molecules can bind with the dopamine functionalities' amine and hydroxyl groups via hydrogen bonding or electrostatic interaction [39]. In general, the quantity of drug encapsulated into the drug delivery carrier system and released into specified areas is thought to be essential for

increasing therapeutic efficacy while avoiding adverse effects on normal tissues. Therefore, the FeNP@MSHC NPs may be useful for regulated drug loading and release via an electrostatic repulsive force between the protonated drugs and drug carriers in response to intracellular pH conditions (Scheme 1, step 7).

### 3.3. Drug Release from the FeNP@MSHC/Dox NPs

Various stimuli such as (i) varied pH (pH 7.4 and 5.0); (ii) different temperatures such as room temperature (25 °C), physiological body temperature (37 °C), and magnetic hyperthermia temperature (42 °C); and the combined pH and temperature (pH 7.4/42 °C and pH 5.0/42 °C, were explored to access the in vitro drug release performance of the FeNP@MSHC/Dox NPs. Figure 4a depicts the Dox delivery performance of the FeNP@MSHC/Dox NPs at varied pH (pH 7.4 and 5.0) conditions.

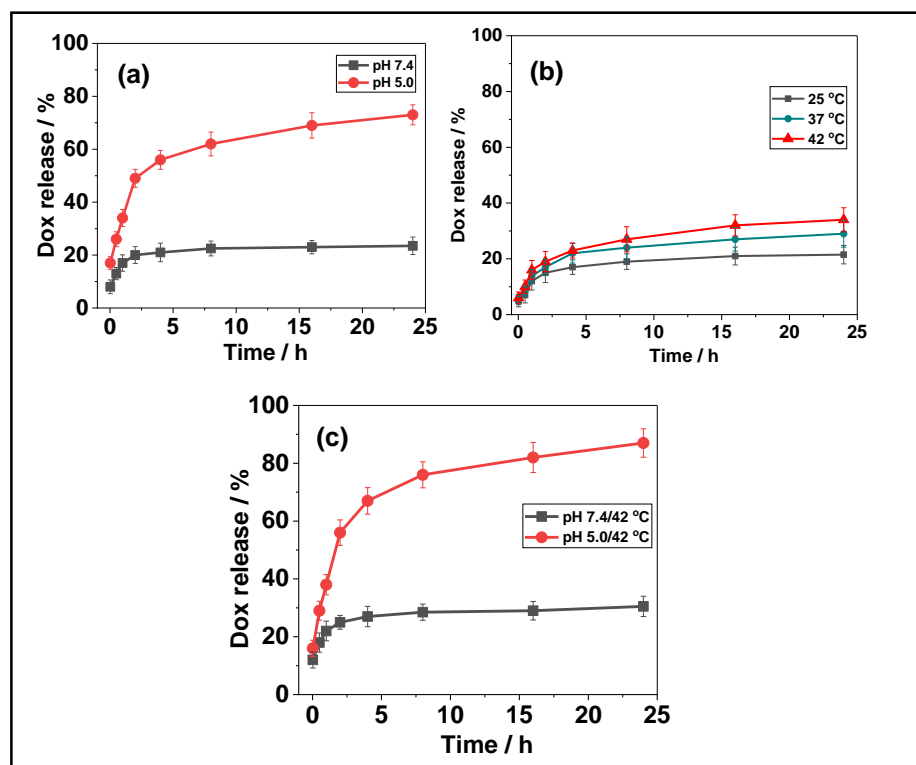


**Figure 4.** In vitro Dox release from the FeNP@MSHC/Dox NPs at (a) different pH; (b) different temperature; (c) the combined pH and temperature.

The cumulative Dox release at pH 7.4 was approximately 23.5% in 24 h, as shown in Figure 4a. Dox release, on the other hand, was significantly increased to approximately ~73% under acidic pH (pH 5.0) conditions in a 24 h period (Figure 4a). The drug release results show that the majority of the drug was preserved inside the mesopores under a physiological pH environment. Because of the hydrogen bonding/electrostatic interaction between drug molecules and drug binding sites, such as hydroxyl and amine groups in the dopamine-silane functionalities present in the FeNP@MSHC/Dox NPs, drug release was significantly reduced. When the pH of the release media was decreased to pH 5.0, the drug-binding organic functional sites present in the FeNP@MSHC/Dox NPs were protonated, resulting in an electrostatic repulsive force between the protonated drug and the drug-binding functional groups (Figure 4a). As a result, the Dox-loaded FeNP@MSHC/Dox NPs demonstrated improved Dox release (~73%) at pH 5.0 (Scheme 1, step 7) (Table 2).

**Table 2.** PH and temperature-responsive drug delivery from the FeNP@MSHC/Dox NPs.

pH	Release Efficiency (%)
7.4	23.5
5.0	52.4
7.4/25 °C	21.5
7.4/42 °C	34
7.4/42 °C	34
5.0/42 °C	87

To evaluate the temperature-responsive behavior of the prepared FeNP@MSHC NPs, various temperature conditions such as room temperature (25 °C), physiological body temperature (37 °C), and magnetic hyperthermia temperature (42 °C), were studied. Figure 4b depicts the temperature-responsive Dox release performance of the FeNP@MSHC/Dox NPs at varied temperatures (25 °C, 37 °C, and 42 °C). As shown in Figure 4b, only a minimal quantity of Dox (~21.5%) was released in 24 h at 25 °C. The Dox release, on the other hand, was slightly raised to about 28.7% and ~34% at 37 °C and 42 °C, indicating that higher temperature stimuli can somewhat increase the Dox release from the FeNP@MSHC/Dox NPs. Furthermore, the Dox release was tested under combined pH and temperature conditions (pH 7.4/42 °C and 5.0/42 °C). As displayed in Figure 4c, at pH 7.4/42 °C, approximately ~30.5% of Dox release was determined. At pH 5.0/42 °C, the FeNP@MSHC/Dox NPs demonstrated an increased Dox release of approximately ~87%. Dox release was dramatically enhanced when compared to Dox release only under pH and temperature conditions (Figure 4c). The findings suggest that a combination of pH and temperature stimuli is important in releasing drugs from the FeNP@MSHC/Dox NPs' mesopore channels. The protonation of drug binding sites is caused by pH stimuli. Furthermore, temperature stimuli are responsible for increasing drug solubility and drug diffusion out of the FeNP@MSHC/Dox NPs' mesopore channels. As a consequence, the combined acidic pH and temperature (pH 5.0/42 °C) stimuli considerably enhanced Dox release compared to either acidic pH or temperature stimuli alone [40] (Table 2).

### 3.4. In Vitro Cytotoxicity Study

Using MDA-MB-231 cells, the MTT assay analysis was performed to evaluate the biocompatibility of the prepared FeNP@MSHC NPs and the Dox-loaded FeNP@MSHC/Dox NPs at different sample concentrations (50, 100, 150, 200, and 250 µg/mL). As seen in Figure 5A, at the tested doses, the FeNP@MSHC NPs without Dox loading demonstrated >~90% cell viability to MDA-MB-231 cells. This finding implies that the prepared FeNP@MSHC NPs are biocompatible. However, the Dox-loaded FeNP@MSHC/Dox NPs and free Dox exhibited concentration-dependent cytotoxicity, with more than ~90% of the cells being killed when treated with FeNP@MSHC/Dox NPs at a concentration of about ~250 µg/mL. Similarly, the same concentration of pure Dox caused ~78% cytotoxicity in MDA-MB-231 cells. The cytotoxicity increased as the FeNP@MSHC/Dox NPs concentrations increased (Figure 5B). As demonstrated in Figure 5B, the Dox-loaded FeNP@MSHC/Dox NPs had a greater killing effect (>~90%) than the same concentration of pure Dox. This might be due to the slow and prolonged release of Dox molecules from the FeNP@MSHC/Dox NPs' mesopore channels, which results in higher cell-killing efficiency. The hydrogen bonding/electrostatic interaction between the Dox molecules and the drug binding amine and hydroxyl groups in the dopamine-silane functionality found in the FeNP@MSHC/Dox NPs controls the drug release behavior [41]. In general, free drug molecules enter cells by the passive diffusion process, whereas FeNP@MSHC/Dox NPs are internalized via the endocytosis mechanism, and therefore the loaded drugs are slowly released from the FeNP@MSHC/Dox NPs. The experimental investigation results show that Dox-loaded FeNP@MSHC/Dox NPs may significantly decrease cancer cell growth, and therefore the FeNP@MSHC NPs might be used as a magnetically directed drug delivery system for target cancer treatment.

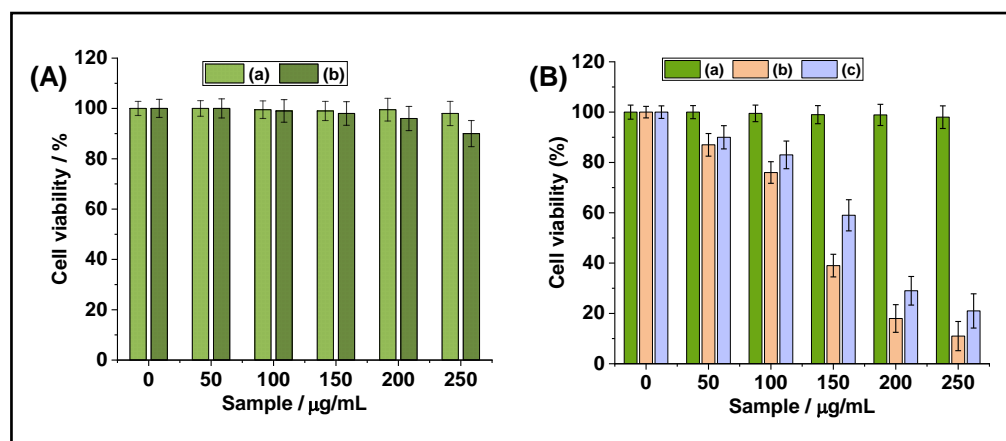


**Figure 5.** (A) In vitro biocompatibility of (a) control MDA-MB-231 cells; (b) FeNP@MSHC NPs without Dox loading, at different concentrations. (B) In vitro cytotoxicity of (a) control MDA-MB-231 cells; (b) FeNP@MSHC/Dox NPs; and (c) pure Dox sample, at different sample concentrations.

### 3.5. In Vitro Cell-Uptake Experiments

MDA-MB-231 cells were used to evaluate the in vitro cellular uptake behavior of the prepared FeNP@MSHC/Dox NPs. Fluorescence microscopy was used to examine the cell uptake of the FeNP@MSHC/Dox NPs. To conduct this experiment, FeNP@MSHC/Dox NPs (10 µg/mL) were dispersed in PBS solution and exposed to MDA-MB-231 cells for 4 h. After 4 h of incubation, the cells were rinsed with PBS solution and examined under a fluorescence microscope. Figure 6a showed only control cells without sample treatment and shows no visible fluorescence signals, however, the FeNP@MSHC/Dox NPs treated cells produced a strong red signal (Figure 6b), indicating that the FeNP@MSHC/Dox NPs were internalized into the MDA-MB-231 cells. The cell uptake of the FeNP@MSHC/Dox NPs was observed at different time intervals, and the intensity of the red signal increased inside the cells with respect to time, which confirmed that the release of Dox inside the cells increased with time (Figure 6c). This experimental finding suggests that the FeNP@MSHC/Dox NPs might be applied for pH- and temperature-stimuli-responsive drug delivery in cancer therapy.

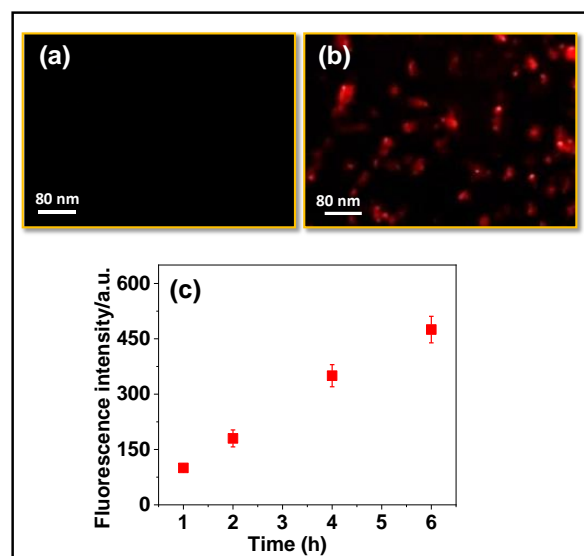


**Figure 6.** Fluorescence microscopy images of MDA-MB-231 cells; (a) only control cells without exposing FeNP@MSHC/Dox NPs; (b) the cells exposed with the Dox loaded FeNP@MSHC/Dox NPs. The red signals indicate the released Dox inside the MDA-MB-231 cells. (c) Fluorescence intensity of the released Dox from the FeNP@MSHC/Dox NPs at different time intervals. Scale bar = 80 µm.

#### 4. Conclusions

In conclusion, the magnetic iron oxide nanoparticle-modified mesoporous silica composite nanoparticles, FeNP@MSHC NPs, were synthesized using sol-gel co-condensation, metal–ligand complex coordination, and chemical reduction methods. Magnetic iron oxide nanoparticles were produced on the outer silica surfaces using this technique. The FeNP@MSHC NPs developed had a high surface area and large pore size and volume. The system demonstrated significant drug-loading capacity and pH- and temperature-responsive drug-release behavior due to the presence of integrated dopamine-silane functionalities in the FeNP@MSHC NPs. Furthermore, the MTT assay analysis findings show that the FeNP@MSHC NPs are biocompatible, and the in vitro cell-uptake study results show that the FeNP@MSHC NPs can be internalized into MDA-MB-231 cells. According to the findings, it is possible to conclude that the prepared FeNP@MSHC NPs might be used as a pH- and temperature-stimuli-responsive drug carrier to deliver anticancer drugs in cancer therapy applications.

**Author Contributions:** Conceptualization, methodology, formal analysis, M.S. and K.T.; validation, S.K. and L.G.; data curation, M.S. and K.T.; writing—original draft preparation, K.T., M.S., T.T.V.P. and S.D.; writing—review and editing, supervision, project administration, funding acquisition, S.-C.K. All authors have read and agreed to the published version of the manuscript.

**Funding:** This research was supported by the Basic Science Research Program through the National Research Foundation of Korea (NRF) funded by the Ministry of Education (2020R1I1A3052258). In addition, the work was also supported by the Technology Development Program (S3060516), funded by the Ministry of SMEs and Startups (MSS, Republic of Korea) in 2021.

**Data Availability Statement:** Not applicable.

**Conflicts of Interest:** The authors declare no conflict of interest.

#### References

- Baig, N.; Kammakam, I.; Falath, W. Nanomaterials: A review of synthesis methods, properties, recent progress, and challenges. *Mater. Adv.* **2021**, *2*, 1821–1871.
- Harish, V.; Tewari, D.; Gaur, M.; Yadav, A.B.; Swaroop, S.; Bechelany, M.; Barhoum, A. Review on Nanoparticles and Nanostructured Materials: Bioimaging, Biosensing, Drug Delivery, Tissue Engineering, Antimicrobial, and Agro-Food Applications. *Nanomaterials* **2022**, *12*, 457. [\[PubMed\]](#)
- Bayda, S.; Adeel, M.; Tuccinardi, T.; Cordani, M.; Rizzolia, F. The History of Nanoscience and Nanotechnology: From Chemical–Physical Applications to Nanomedicine. *Molecules* **2020**, *25*, 112.
- Khan, I.; Saeed, K.; Khan, I. Nanoparticles: Properties, applications and toxicities. *Arab. J. Chem.* **2019**, *12*, 908–931.
- Navya, P.N.; Daima, H.K. Rational engineering of physicochemical properties of nanomaterials for biomedical applications with nanotoxicological perspectives. *Nano Conver.* **2016**, *3*, 1. [\[CrossRef\]](#)
- Chandrakala, V.; Aruna, V.; Angajala, G. Review on metal nanoparticles as nanocarriers: Current challenges and perspectives in drug delivery systems. *Emergent Mater.* **2022**, *5*, 1593–1615. [\[CrossRef\]](#)
- Chavali, M.S.; Nikolova, M.P. Metal oxide nanoparticles and their applications in nanotechnology. *SN Appl. Sci.* **2019**, *1*, 607. [\[CrossRef\]](#)
- Shen, Y.; Zhang, L.; Wang, K.; Li, X.; Li, J.; Zhang, S.; Zhao, H.; Jiang, X.; Guan, W.; Yang, L. Bio-mediated synthesis—A sustainable strategy for nanomaterials preparation: A comprehensive bibliometric review. *Nanoselect* **2021**, *2*, 2275–2290.
- Chircov, C.; Spoiala, A.; Puan, C.; Craciun, L.; Ficai, D.; Ficai, A.; Andronescu, E.; Turculet, S.C. Mesoporous Silica Platforms with Potential Applications in Release and Adsorption of Active Agents. *Molecules* **2020**, *25*, 3814.
- Wang, D.; Chen, X.; Feng, J.; Sun, M. Recent advances of ordered mesoporous silica materials for solid-phase extraction. *J. Chromatogr. A* **2022**, *1675*, 463157.
- Feng, Y.; Liao, Z.; Li, M.; Zhang, H.; Li, T.; Qin, X.; Li, S.; Wu, C.; You, F.; Liao, X.; et al. Mesoporous Silica Nanoparticles-Based Nanoplatfroms: Basic Construction, Current State, and Emerging Applications in Anticancer Therapeutics. *Adv. Healthcare Mater.* **2022**, *18*, 2201884. [\[CrossRef\]](#)
- Prabha, S.; Durgalakshmi, D.; Rajendran, S.; Lichtfouse, E. Plant-derived silica nanoparticles and composites for biosensors, bioimaging, drug delivery and supercapacitors: A review. *Environ. Chem. Lett.* **2021**, *19*, 1667–1691. [\[CrossRef\]](#) [\[PubMed\]](#)
- Guimaraes, R.; Rodrigues, C.; Moreira, A.F.; Correia, I. Overview of stimuli-responsive mesoporous organosilica nanocarriers for drug delivery. *Pharmacol. Res.* **2020**, *155*, 104742. [\[PubMed\]](#)

14. Park, S.S.; Moorthy, M.S.; Ha, C.S. Periodic mesoporous organosilicas for advanced applications. *NPG Asia Mater.* **2014**, *6*, e96. [[CrossRef](#)]
15. Moorthy, M.S.; Park, S.S.; Fuping, D.; Hong, S.-H.; Selvaraj, M.; Ha, C.S. Step-up synthesis of amidoxime-functionalised periodic mesoporous organosilicas with an amphoteric ligand in the framework for drug delivery. *J. Mater. Chem.* **2012**, *22*, 9100–9108.
16. Moorthy, M.S.; Hoang, G.; Subramanian, B.; Bui, N.Q.; Panchanathan, M.; Mondal, S.; Tuong, V.P.T.; Kim, H.; Oh, J. Prussian blue decorated mesoporous silica hybrid nanocarriers for photoacoustic imaging-guided synergistic chemo-photothermal combination therapy. *J. Mater. Chem. B* **2018**, *6*, 5220–5233.
17. Yu, L.; Chen, Y.; Lin, H.; Du, W.; Chen, H.; Shi, J. Ultrasmall mesoporous organosilica nanoparticles: Morphology modulations and redox-responsive biodegradability for tumor-specific drug delivery. *Biomaterials* **2018**, *161*, 292–305.
18. Ashouri, A.; Samadi, S.; Nasiri, B.; Bahrami, Z. Iron-based nanomaterials used as magnetic mesoporous nanocomposites to catalyze the preparation of N-sulfonylimines. *Comptes Rendus Chim.* **2019**, *22*, 549–559.
19. Tran, H.-V.; Ngo, N.M.; Medhi, R.; Srinoi, P.; Liu, T.; Rittikulsittichai, S.; Lee, T.R. Multifunctional Iron Oxide Magnetic Nanoparticles for Biomedical Applications: A Review. *Materials* **2022**, *15*, 503. [[CrossRef](#)]
20. Nemec, S.; Kralj, S. A Versatile Interfacial Coassembly Method for Fabrication of Tunable Silica Shells with Radially Aligned Dual Mesopores on Diverse Magnetic Core Nanoparticles. *ACS Appl. Mater. Interfaces* **2021**, *13*, 1883–1894.
21. Chang, Z.; Wang, Z.; Shao, D.; Yue, J.; Xing, H.; Li, L.; Ge, M.; Li, M.; Yan, H.; Hu, H.; et al. Shape Engineering Boosts Magnetic Mesoporous Silica Nanoparticle-Based Isolation and Detection of Circulating Tumor Cells. *ACS Appl. Mater. Interfaces* **2018**, *10*, 10656–10663. [[PubMed](#)]
22. Moorthy, M.S.; Subramanian, B.; Panchanathan, M.; Mondal, S.; Kim, H.; Lee, K.D.; Oh, J. Fucoidan-coated core-shell magnetic mesoporous silica nanoparticles for chemotherapy and magnetic hyperthermia-based thermal therapy applications. *New J. Chem.* **2017**, *41*, 15334–15346.
23. Moorthy, M.S.; Kim, H.-B.; Bae, J.-H.; Kim, S.-H.; Ha, C.S. Design of core-shell magnetic mesoporous silica hybrids for pH and UV light stimuli-responsive cargo release. *RSC Adv.* **2016**, *6*, 29106–29115.
24. Zhu, N.; Ji, H.; Yu, P.; Niu, J.; Farooq, M.U.; Akram, M.W.; Udego, I.O.; Li, H.; Niu, X. Surface Modification of Magnetic Iron Oxide Nanoparticles. *Nanomaterials* **2018**, *8*, 810. [[CrossRef](#)]
25. El-Boubbou, K.; Ali, R.; Al-Zahrani, H.; Trivilegio, T.; Alanazi, A.H.; Khan, A.L.; Boudjelal, M.; Alkushi, A. Preparation of iron oxide mesoporous magnetic microparticles as novel multidrug carriers for synergistic anticancer therapy and deep tumor penetration. *Sci. Rep.* **2019**, *9*, 9481. [[CrossRef](#)] [[PubMed](#)]
26. Bruckmann, F.S.; Nunes, F.B.; Salles, T.R.; Franco, C.; Cadona, F.C.; Rhoden, C.R.B. Biological Applications of Silica-Based Nanoparticles. *Magnetochemistry* **2022**, *8*, 131. [[CrossRef](#)]
27. Yu, X.; Wang, L.; Li, K.; Mi, Y.; Li, Z.; Wu, D.; Sun, F.; He, S.; Zeng, H. Tuning dipolar effects on magnetic hyperthermia of Zn<sub>0.3</sub>Fe<sub>2.7</sub>O<sub>4</sub>/SiO<sub>2</sub> nanoparticles by silica shell. *J. Magn. Magn. Mater.* **2021**, *521*, 167483.
28. Zhang, J.; Lin, Y.; Lin, Z.; Wei, Q.; Quan, J.; Ruan, R.; Jiang, X.; Hou, L.; Song, J.; Ding, J.; et al. Stimuli-Responsive Nanoparticles for Controlled Drug Delivery in Synergistic Cancer Immunotherapy. *Adv. Sci.* **2021**, *9*, 2103444.
29. Hershberger, K.K.; Gauger, A.J.; Bronstein, L.M. Utilizing Stimuli Responsive Linkages to Engineer and Enhance Polymer Nanoparticle-Based Drug Delivery Platforms. *ACS Appl. Bio. Mater.* **2021**, *4*, 4720–4736.
30. Au, J.L.-S.; Yeung, B.Z.; Wientjes, M.G.; Lu, Z.; Wientjes, M.G. Delivery of cancer therapeutics to extracellular and intracellular targets: Determinants, barriers, challenges and opportunities. *Adv. Drug Deliv. Rev.* **2016**, *97*, 280–301. [[PubMed](#)]
31. Ponomareva, S.; Joisten, H.; Francois, T.; Naud, C.; Morel, R.; Hou, Y.; Myer, T.; Joumard, I.; Dieny, B.; Carriere, M. Magnetic particles for triggering insulin release in INS-1E cells subjected to a rotating magnetic field. *Nanoscale* **2022**, *14*, 13274–13283. [[PubMed](#)]
32. Moorthy, M.S.; Park, J.-H.; Bae, J.-H.; Kim, S.-H.; Ha, C.S. Mesoporous organosilica hybrids with a tunable amphoteric framework for controlled drug delivery. *J. Mater. Chem. B* **2014**, *2*, 6487–6499. [[PubMed](#)]
33. Cui, R.; Zhang, K.; Wu, X.; Zhang, H.; Wang, C. Determination of Fe<sup>3+</sup> upon Special “Upconversion Luminescence” of Dopamine. *ACS Omega* **2019**, *4*, 9918–9924. [[PubMed](#)]
34. Kumar, P.; Nagarajan, A.; Uchil, P.D. Analysis of Cell Viability by the MTT Assay. *Cold Spring Harb. Protoc.* **2018**, *2018*, pdb-prot095505. [[CrossRef](#)]
35. Gao, J.; Lei, H.; Han, Z.; Shi, Q.; Chen, Y.; Jinag, Y. Dopamine functionalized tannic-acid-templated mesoporous silica nanoparticles as a new sorbent for the efficient removal of Cu<sup>2+</sup> from aqueous solution. *Sci. Rep.* **2017**, *7*, 45215. [[CrossRef](#)]
36. Tian, Z.; Yu, X.; Ruan, Z.; Zhu, M.; Zhu, Y.; Hanagata, N. Magnetic mesoporous silica nanoparticles coated with thermo-responsive copolymer for potential chemo- and magnetic hyperthermia therapy. *Micropor. Mesopor. Mater.* **2018**, *256*, 1–9.
37. Moorthy, M.S.; Seo, D.-J.; Song, H.-J.; Park, S.S.; Ha, C.S. Magnetic mesoporous silica hybrid nanoparticles for highly selective boron adsorption. *J. Mater. Chem. A* **2013**, *40*, 12485–12496.
38. Baeza, A.; Guisasaola, E.; Ruiz-Hernandez, E.; Vallet-Regi, M. Magnetically Triggered Multidrug Release by Hybrid Mesoporous Silica Nanoparticles. *Chem. Mater.* **2012**, *24*, 517–524.
39. Sims, K.R., Jr.; He, B.; Koo, H.; Benoit, D.S.W. Electrostatic Interactions Enable Nanoparticle Delivery of the Flavonoid Myricetin. *ACS Omega* **2020**, *5*, 12649–12659.

40. Farjadian, F.; Rezaeifard, S.; Naeimi, M.; Ghasemi, S.; Mohammadi-Samani, S.; Welland, M.E.; Tayebi, L. Temperature and pH-responsive nano-hydrogel drug delivery system based on lysine-modified poly (vinylcaprolactam). *Int. J. Nanomed.* **2019**, *14*, 6901–6915. [[CrossRef](#)]
41. Saputra, O.A.; Lestari, W.A.; Kurniansyah, V.; Lestari, W.W.; Sugiura, T.; Mukti, R.R.; Martien, R.; Wibowo, F.R. Organically surface engineered mesoporous silica nanoparticles control the release of quercetin by pH stimuli. *Sci. Rep.* **2022**, *12*, 20661. [[CrossRef](#)] [[PubMed](#)]

**Disclaimer/Publisher’s Note:** The statements, opinions and data contained in all publications are solely those of the individual author(s) and contributor(s) and not of MDPI and/or the editor(s). MDPI and/or the editor(s) disclaim responsibility for any injury to people or property resulting from any ideas, methods, instructions or products referred to in the content.